Journal of the American College of Cardiology. 2017; 69(4)

Role of NOD1 in heart failure progression via regulation of Ca^{2+} handling

Almudena Val-Blasco, BsC[a], María Jose G.M. Piedras, PhD[b], Gema Ruiz-Hurtado, PhD[c], Natalia Suarez, PhD[d], Patricia Prieto, PhD[e], Silvia Gonzalez-Ramos, BsC[e], Nieves Gómez-Hurtado, PhD[f], Carmen Delgado, PhD[e], f, Laetitia Pereira, PhD[g], Gemma Benito, BsC[a], Carlos Zaragoza, PhD[b], Nieves Domenech, PhD[h], María Generosa Crespo-Leiro, MD, PhD[d], Daniel Vasquez-Echeverri, PhD[d], Gabriel Nuñez, MD, PhD[i], Eduardo Lopez-Collazo, PhD[a], j, Lisardo Boscá, PhD[e], María Fernández-Velasco, PhD[a]

[a] *Innate Immune Response Group, Instituto de Investigación La Paz, La Paz University Hospital, Madrid, Spain*
[b] *Department of Cardiology, University Hospital Ramón y Cajal/University Francisco de Vitoria, Madrid, Spain*
[c] *Unidad de Hipertensión, Instituto de Investigación i+12 Hospital Universitario 12 de Octubre, Madrid, Spain*
[d] *Cardiology Department, Instituto de Investigación Biomédica de A Coruña, Complexo Hospitalario Universitario de A Coruña, Servicio Gallego de Salud, Universidade da Coruña, Coruña, Spain*
[e] *Instituto de Investigaciones Biomédicas Alberto Sols, Consejo Superior de Investigaciones Científicas, Madrid, Spain*
[f] *Departament of Pharmacology, School of Medicine, Complutense University, Madrid, Spain*
[g] *Department of Pharmacology, University of California, Davis, Davis, California*
[h] *Biobanco A Coruña, Complexo Hospitalario Universitario A Coruña e Instituto de Investigación Biomédica, Coruña, Spain*
[i] *Department of Pathology and Comprehensive Cancer Center, University of Michigan Medical School, Ann Arbor, Michigan*
[j] *Center for Biomedical Research Network, Centro de Investigación Biomédica en Red de Enfermedades Respiratorias, Madrid, Spain*

Abstract

Background

Heart failure (HF) is a complex syndrome associated with a maladaptive innate immune system response that leads to deleterious cardiac remodeling. However, the underlying mechanisms of this syndrome are poorly understood. Nucleotide-binding oligomerization domain-containing protein 1 (NOD1) is a newly recognized innate immune sensor involved in cardiovascular diseases.

Objectives

This study evaluated the role of NOD1 in HF progression.

Methods

NOD1 was examined in human failing myocardium and in a post-myocardial infarction (PMI) HF model evaluated in wild-type (wt-PMI) and *Nod1*$^{-/-}$ mice (*Nod1*$^{-/-}$-PMI).

Results

The NOD1 pathway was up-regulated in human and murine failing myocardia. Compared with wt-PMI, hearts from *Nod1*$^{-/-}$-PMI mice had better cardiac function and attenuated structural remodeling. Ameliorated cardiac function in *Nod1*$^{-/-}$-PMI mice was associated with prevention of Ca^{2+} dynamic impairment linked to HF, including smaller and longer intracellular Ca^{2+} concentration transients and a lesser sarcoplasmic reticulum Ca^{2+} load due to a down-regulation of the sarcoplasmic reticulum Ca^{2+}-adenosine triphosphatase pump and by augmented levels of the Na^{+}/Ca^{2+} exchanger. Increased diastolic Ca^{2+} release in wt-PMI cardiomyocytes was related to hyperphosphorylation of ryanodine receptors, which was blunted in *Nod1*$^{-/-}$-PMI cardiomyocytes. Pharmacological blockade of NOD1 also prevented Ca^{2+} mishandling in wt-PMI mice. *Nod1*$^{-/-}$-PMI mice showed significantly fewer ventricular arrhythmias and lower mortality after isoproterenol administration. These effects were associated with lower aberrant systolic Ca^{2+} release and with a prevention of the hyperphosphorylation of ryanodine receptors under isoproterenol administration in *Nod1*$^{-/-}$-PMI mice.

Conclusions

NOD1 modulated intracellular Ca^{2+} mishandling in HF, emerging as a new target for HF therapy.

Key Words
Calcium; Cardiac arrhythmia; Cardiac dysfunction; Innate immune system; Myocardial infarction; Ryanodine receptor

Abbreviations and Acronyms
$[Ca^{2+}]_i$, intracellular Ca^{2+} concentration; CaMKII, calcium/calmodulin-dependent protein kinase II; CMR, cardiac magnetic resonance; EC, excitation-contraction; EF, ejection fraction; HF, heart failure; I_{CaL}, triggered Ca^{2+} current through L-type calcium channel; iE-DAP, lauroyl γ-D-glutamyl-meso-diaminopimelic acid; MI, myocardial infarction; NCX, Na^+/Ca^{2+} exchanger; NLR, nucleotide-binding oligomerization domain-like receptor; NOD1, nucleotide-binding oligomerization domain-containing protein 1; PKA, protein kinase A; PMI, post-myocardial infarction; RIP2, receptor-interacting protein 2; RyR, ryanodine receptor; SCR, spontaneous Ca^{2+} release; SERCA, sarcoplasmic reticulum Ca^{2+}-adenosine triphosphatase 2a pump; SR, sarcoplasmic reticulum; VT, ventricular tachycardia; wt, wild type

Heart failure (HF) occurs when the heart is unable to maintain cardiac output at normal filling pressures. HF is among the leading causes of death and hospitalization in Western countries and constitutes a significant economic burden (1). Despite advances in treatment, the prognosis for HF patients remains poor, underscoring the need for new therapeutic options.

HF is characterized by increased cardiac activation of the innate immune system, independent of disease etiology (2,3). Although the innate immune system appears to influence clinical outcomes in HF patients, use of anti-inflammatory drugs has not yielded the expected benefits in clinical trials (4). Given its complexity, the design of new anti-inflammatory HF treatments requires a detailed understanding of how the innate immune system influences the development and progression of the disease.

As the first line of host defense against pathogens or environmental damage, the innate immune system triggers a proinflammatory response when challenged. Although essential for homeostatic responses and tissue repair, chronic activation of the cardiac innate immune system results in deleterious cardiac remodeling. The innate immune system is mainly regulated by 2 families of receptors: toll-like receptors and nucleotide-binding oligomerization domain-like receptors (NLR). Toll-like receptors are the best characterized innate immune receptors in the cardiovascular system (3,4); much less information is available on NLR, although they are a current area of active research (5). Nucleotide-binding oligomerization domain-containing protein 1 (NOD1), a member of the NLR family, has recently been implicated in several cardiovascular pathologies, including atherosclerosis and diabetic cardiomyopathy (6,7). NOD1 is expressed in murine heart and, on activation, undergoes a conformational change that promotes the activation of receptor-interacting protein 2 (RIP2), ultimately triggering the proinflammatory response. Recent findings showed that selective activation of NOD1 induces cardiac dysfunction by impairing excitation-contraction (EC) coupling (8). In the heart, EC coupling depends primarily on a mechanism called Ca^{2+}-induced Ca^{2+} release, which is initiated by an action potential in the cardiomyocytes that fires a small influx of Ca^{2+} via sarcolemma L-type Ca^{2+} channels. This triggers a large release of Ca^{2+} from the sarcoplasmic reticulum (SR) through ryanodine receptors (RyR), resulting in an increased intracellular Ca^{2+} concentration ($[Ca^{2+}]_i$) that activates myofilaments, prompting cell contraction. Relaxation is achieved by pumping Ca^{2+} to the SR via sarcoplasmic reticulum Ca^{2+}-adenosine triphosphatase 2a (SERCA), whose activity is regulated by phospholamban and across the plasma membrane through the Na^+/Ca^{2+} exchanger (NCX). Impairment of EC coupling is well documented in experimental and human HF. Importantly, Ca^{2+} mishandling linked to HF is closely related to depressed cardiac function and cardiac arrhythmia development (9).

Because NOD1 activation in wild-type (wt) myocytes impairs EC coupling in a manner similar to that described in HF (8), we analyzed whether NOD1 participates in HF progression.

METHODS

All human and animal studies were performed with the permission of A Coruña and La Paz Hospitals on human ethics and animal policy and welfare following recommendations of the Spanish and European guidelines (Ref. 2010/63/EU).

As previously described (8), male *Nod1*$^{-/-}$ mice on a C57BL/6J (6B; 129P2- NOD1^{tm1Nnz}/J) background were used (provided by G.N.), and C57BL/6J (Jackson Laboratory, Bar Harbor, Maine) wt mice were used as control specimens. Expanded methods are presented in the Online Appendix.

RESULTS

Immunohistochemical analysis of myocardial tissue obtained from HF patients and unused healthy myocardia from transplant donors (healthy hearts) demonstrated higher levels of NOD1 in HF than in healthy heart samples, which were localized to the rod-shaped cardiomyocyte population (Figure 1A; immunostaining control specimens are presented in Online Figure 1). Immunoblots show higher protein levels of NOD1, its specific adaptor RIP2, and the proinflammatory mediator tumor necrosis factor-α in HF versus healthy heart tissue (Figures 1B and 1C). We evaluated the relationship among cardiac output, ejection fraction (EF), and NOD1 levels. A significant negative correlation was found between NOD1 and cardiac output or EF in HF patients (Figures 1D and 1E).

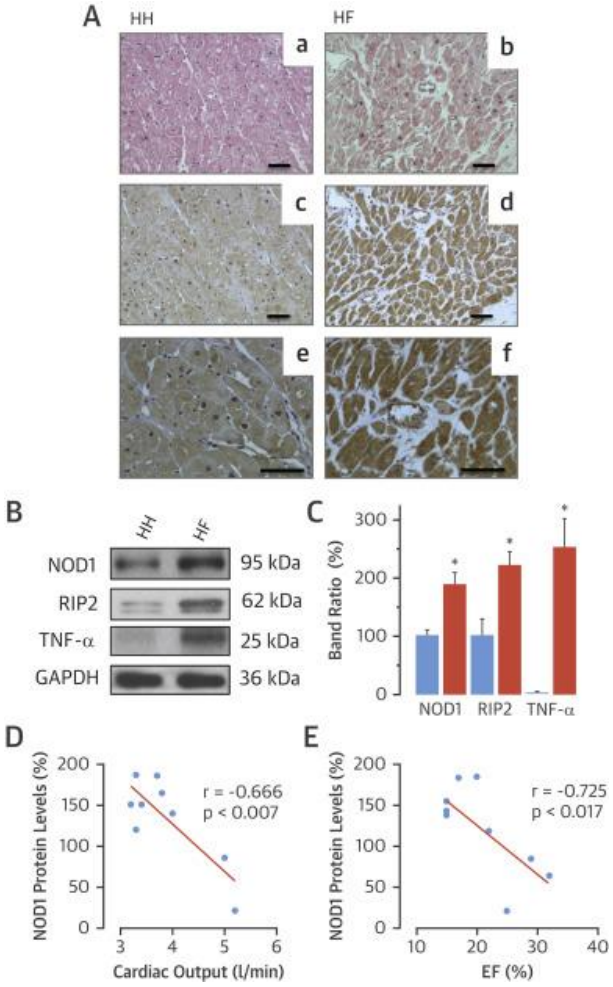

Figure 1. NOD1 Overexpressed in Failing Myocardium
(A) Representative hematoxylin and eosin–stained sections of healthy myocardium (HH) **(a)** and heart failure (HF) myocardium **(b)** (original magnification: 10×). **(c to f)** Immunohistochemistry staining of transversal sections demonstrated that nucleotide-binding oligomerization domain-containing protein 1 (NOD1) is higher in cardiomyocytes of HF versus HH (original magnification: 10× **[c, d]**; 20× **[e, f]**). Bars = 100 μm. **(B, C)** Representative Western blots of NOD1, receptor-interacting protein 2 (RIP2), tumor necrosis factor-α (TNF-α), and glyceraldehyde 3-phosphate dehydrogenase (GAPDH) from HH (n = 7; **blue bars**) and HF (n = 12; **orange bars**) samples, and quantification of Western blots (mean ± SEM). *$p < 0.05$ versus HH. **(D, E)** Negative correlation between NOD1 protein and cardiac output or ejection fraction (EF) in HF patients. Analysis was performed using the Pearson correlation. A linear regression of the data is shown.

We next examined NOD1 protein levels in cardiac tissue from mice with HF induced by myocardial infarction (MI). NOD1, RIP2, and tumor necrosis factor-α levels were higher in whole hearts of HF-induced wild-type mice at 6 weeks post-myocardial infarction (wt-PMI) than in equivalent sham-operated wt mice (Figures 2A and 2B). Six weeks after MI, mice were analyzed for cardiac function and morphometries. Survival was not different between the wt-PMI and *Nod1*$^{-/-}$-PMI mice (not shown). Echocardiography recordings showed that EF (Figure 2C) and fractional shortening (Figure 2D) were significantly lower in wt-PMI mice ($p < 0.001$), whereas *Nod1*$^{-/-}$-PMI mice exhibited improved EF and fractional shortening parameters (Figures 2C and 2D). Cardiac magnetic resonance (CMR) analysis supported the prevention of MI-induced cardiac dysfunction in *Nod1*$^{-/-}$-PMI mice (Figure 2E, Table 1). Furthermore, CMR after gadolinium enhancement showed that hearts of *Nod1*$^{-/-}$-PMI mice had significantly smaller infarcts than did wt-PMI mice (Figure 2F). Additionally, wt-PMI mice treated for

6 weeks with the NOD1 inhibitor nodinitib-1 (10) also exhibited significantly better EF and fractional shortening values after PMI (Online Figure 2).

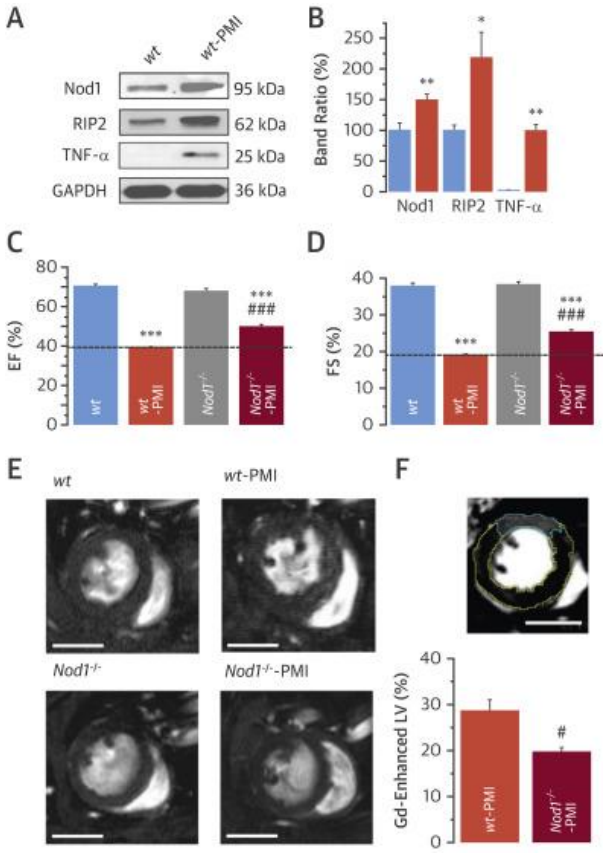

Figure 2. Effects of NOD1 Absence: Murine HF Model

(A, B) Representative Western blots of NOD1, RIP2, TNF-α, and GAPDH from cardiac tissue of wild-type (wt; **blue bars**) (n = 5) and wild-type post-myocardial infarction (wt-PMI; **orange bars**) (n = 6) mice, and quantification of Western blots (mean ± SEM). **(C, D)** Mean values of the EF and fractional shortening (FS) in wt (n = 3) and *Nod1*$^{-/-}$ (n = 3) mice before and 6 weeks PMI. **(E)** Representative 2-chamber short-axis cardiac magnetic resonance images at the end of diastole. **(F)** An example of late-enhanced recordings 20 to 40 min following application of gadolinium (Gd)-based contrast agent obtained in wt-PMI mice with mean values of quantification in wt (n = 5) and *Nod1*$^{-/-}$ (n = 7) mice 6 weeks PMI. Mean ± SEM; Bars = 3 mm. *p < 0.05, **p < 0.01, ***p < 0.001 versus wt; $^{\#}$p < 0.05, $^{\#\#\#}$p < 0.001 versus wt-PMI. LV = left ventricle; other abbreviations as in Figure 1.

Table 1. Macroscopic and Cellular Parameters

	Sham-Operated		PMI	
	wt	*Nod1*$^{-/-}$	wt	*Nod1*$^{-/-}$
Heart rate, beats/min	392.34 ± 5.34 (4)	415.99 ± 20.04 (4)	394.10 ± 15.70 (6)	428.91 ± 26.99 (8)
SV, μl	38.80 ± 1.10 (4)	31.90 ± 1.03 (4)	27.61 ± 2.73* (6)	35.01 ± 1.50† (8)
CO, ml/min	15.24 ± 0.43 (4)	13.87 ± 0.59 (4)	10.18 ± 1.00* (6)	14.98 ± 0.64‡ (8)
LVWTD, mm	0.57 ± 0.01 (4)	0.52 ± 0.00 (4)	0.80 ± 0.06§ (6)	0.62 ± 0.03† (8)
IVSWTD, mm	0.43 ± 0.07 (4)	0.42 ± 0.02 (4)	0.55 ± 0.03§ (6)	0.45 ± 0.03 (8)
HW, mg	211.13 ± 6.60 (12)	200.90 ± 10.80 (9)	257.1 ± 7.80§ (17)	217.00 ± 11.30† (17)
Body weight, g	26.83 ± 0.70 (12)	26.70 ± 1.90 (9)	29.20 ± 0.80 (17)	30.00 ± 11.30 (17)
TL, mm	21.80 ± 0.21 (12)	21.33 ± 0.30 (9)	21.50 ± 0.42 (17)	21.9 ± 0.20 (17)
HW/TL, mg/mm	9.90 ± 0.30 (12)	9.38 ± 0.46 (9)	12.07 ± 0.36‖ (17)	9.63 ± 0.45‡ (17)
Cell area, μm^2	1,963.50 ± 158.00 (17)	2,033.00 ± 141.70 (17)	4,062.00 ± 193.00‖ (35)	3,215.34 ± 126.00‡¶ (32)

Values are mean ± SEM (n).
CO = cardiac output; HW = heart weight; IVSWTD = interventricular septum thickness at end of diastole; LVWTD = left ventricular free wall thickness at end diastole; *Nod1*$^{-/-}$ = nucleotide-binding oligomerization domain-containing protein 1; PMI = post-myocardial infarction; SV = stroke volume; TL = tibia length; wt = wild type. * $p < 0.01$ versus wt. † $p < 0.05$ versus wt-PMI. ‡ $p < 0.001$ versus wt-PMI. § $p < 0.05$ versus wt. ‖ $p < 0.001$ versus wt. ¶ $p < 0.001$ versus *Nod1*$^{-/-}$.

We next analyzed whether the absence of NOD1 attenuates cardiac hypertrophy development in the HF model. Heart weights and heart weight–tibia length ratio were significantly higher in wt-PMI mice than in noninfarcted wt-mice, although no differences were found in body weights or tibia length among the different groups (Table 1). On CMR analysis, end-diastole left ventricular and interventricular septum thickness were significantly greater in wt-PMI than wt hearts. By contrast, heart weights and heart weight–tibia length ratio in *Nod1*$^{-/-}$-PMI mice were significantly lower than in wt-PMI mice and were very similar to that of noninfarcted *Nod1*$^{-/-}$mice (Table 1). Moreover, hearts from *Nod1*$^{-/-}$-PMI mice did not present an increase in end-diastole left ventricular and interventricular septum thickness (Table 1). Notably, cardiomyocytes isolated from wt-PMI mice had a significantly larger surface area than did wt cardiomyocytes, whereas the surface area of *Nod1*$^{-/-}$-PMI cardiomyocytes was only moderately increased relative to noninfarcted *Nod1*$^{-/-}$ cardiomyocytes (Table 1).

Next, intracellular Ca^{2+} handling was determined in all groups. *Nod1*$^{-/-}$-PMI myocytes showed a significant amelioration of Ca^{2+} mishandling induced by MI, largely by preventing the decrease in amplitude of $[Ca^{2+}]_i$ transients (Figures 3A and 3B), by increasing the decay time constant of $[Ca^{2+}]_i$ transients (Figure 3C), and by reducing the cell contraction detected in wt-PMI myocytes (Figure 3D). We also examined changes in SR Ca^{2+} load by analyzing caffeine-evoked $[Ca^{2+}]_i$ transients, which were weaker in the wt-PMI group than in the wt group (Figure 3E), whereas faster rates of decay were observed in wt-PMI cardiomyocytes: 2.95 ± 0.35 s in wt (n = 13 cells/4 mice) and 2.00 ± 0.20 s in wt-PMI (n = 9 cells/4 mice) ($p < 0.05$). By contrast, caffeine-evoked $[Ca^{2+}]_i$ transients (Figure 3E) and their decay time in cells from *Nod1*$^{-/-}$-PMI mice were very similar to those obtained in *Nod1*$^{-/-}$ cells: 2.60 ± 0.27 s in the *Nod1*$^{-/-}$ group (n = 7 cells/3 mice) and 2.46 ± 0.25 s in the *Nod1*$^{-/-}$-PMI group (n = 10 cells/4 mice).

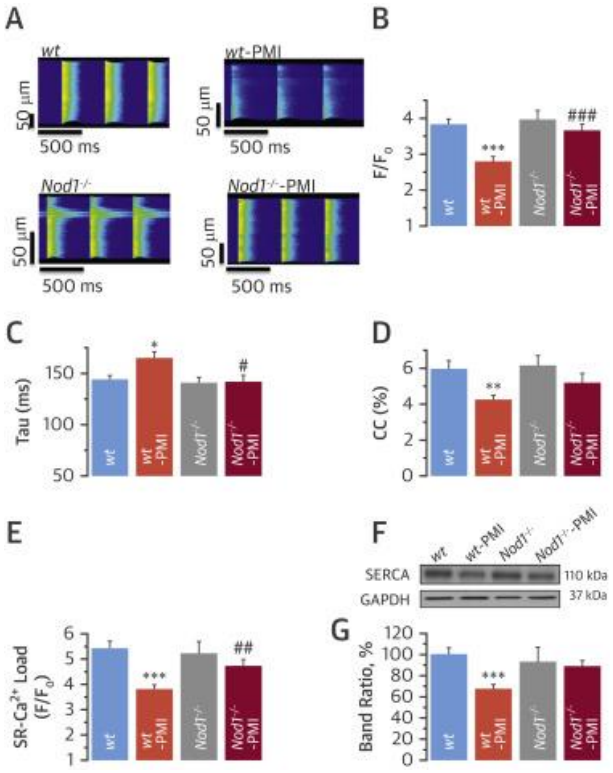

Figure 3. NOD1 Deletion and HF Intracellular Ca^{2+} Mishandling
(A) Representative line-scan confocal images in cells from wt, wt-PMI, *Nod1*$^{-/-}$, and *Nod1*$^{-/-}$-PMI mice. Mean values of **(B)** peak fluorescence $[Ca^{2+}]_i$ transients (F/F_0), **(C)** decay time constant (Tau) and **(D)** cell contraction (CC) in wt (n = 16 cells/5 mice), wt-PMI (n = 33 cells/5 mice), *Nod1*$^{-/-}$ (n = 14 cells/3 mice), and *Nod1*$^{-/-}$-PMI (n = 24 cells/5 mice). **(E)** Mean values of caffeine-evoked $[Ca^{2+}]_i$ transients amplitude (sarcoplasmic reticulum [SR]-Ca^{2+} load, F/F_0) in wt (n = 16 cells/3 mice), wt-PMI (n = 21 cells/4 mice), *Nod1*$^{-/-}$ (n = 12 cells/3 mice), and *Nod1*$^{-/-}$-PMI (n = 19 cells/4 mice). Mean ± SEM. **(F)** Representative immunoblots of SR Ca^{2+}-adenosine triphosphatase 2a (SERCA)/GAPDH from hearts of wt (n = 8), wt-PMI (n = 6), *Nod1*$^{-/-}$ (n = 8), and *Nod1*$^{-/-}$-PMI (n = 6) mice. **(G)** Quantification of Western blots (mean ± SEM) expressed as percentage versus wt. *$p < 0.05$, **$p < 0.01$, ***$p < 0.001$ versus wt; $^{\#}p < 0.05$, $^{\#\#}p < 0.01$, $^{\#\#\#}p < 0.001$ versus wt-PMI. Abbreviations as in Figures 1 and 2.

Additionally, we analyzed the levels of SERCA in all groups. The SERCA in wt-PMI hearts was significantly lower than in wt hearts ($p < 0.001$), whereas in cardiac tissue from *Nod1*$^{-/-}$-PMI mice SERCA levels remained unchanged (Figures 3F and 3G).

NCX protein levels were significantly higher in wt-PMI heart tissue than in equivalent wt samples, whereas similar NCX protein levels were detected in *Nod1*$^{-/-}$-PMI and *Nod1*$^{-/-}$ hearts (Online Figure 3). Supporting these data, pharmacological blockade of NOD1 with nodinitib-1 in wt-PMI mice prevented impairment of systolic Ca^{2+} release and cell contraction and maintained the SR Ca^{2+} load (Online Figure 4).

Diastolic Ca^{2+} release was analyzed by determining Ca^{2+} spark frequency and properties. A similar number of Ca^{2+} sparks was found in cardiomyocytes from all groups (Figure 4A). Ca^{2+} sparks in wt-PMI cardiomyocytes had a larger amplitude and full width at half maximum values than equivalent wt cells, and no change was detected in their full duration at half maximum values. Ca^{2+} spark characteristics were similar in *Nod1*$^{-/-}$-PMI and *Nod1*$^{-/-}$ cardiomyocytes (Online Table 1). Ca^{2+} spark frequencies normalized to the SR Ca^{2+} load obtained in each cell showed similar normalized Ca^{2+} spark frequencies in all groups (Figure 4B). Confirming these data, no differences were found between groups in overall spark-mediated Ca^{2+} leak (Online Figure 5).

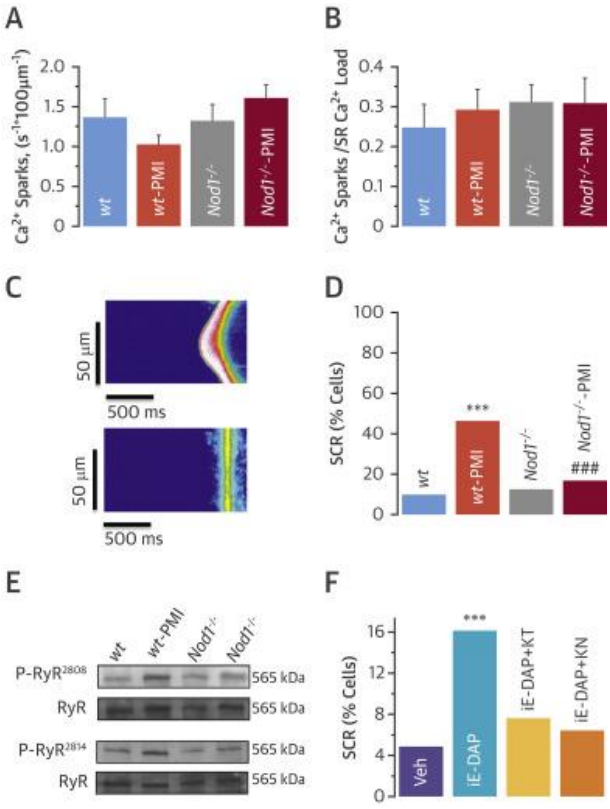

Figure 4. NOD1 Deletion and MI-Induced Diastolic Ca^{2+} Release
Summarized data of mean values of **(A)** Ca^{2+} sparks frequency and **(B)** normalization of Ca^{2+} sparks frequency by SR Ca^{2+} load in wt (n = 20 cells/4 mice), wt-PMI (n = 49 cells/8 mice), *Nod1*$^{-/-}$ (n = 24 cells/4 mice), and *Nod1*$^{-/-}$-PMI (n = 37 cells/8 mice). **(C)** Examples of line-scan images of spontaneous diastolic Ca^{2+} release (SCR) recordings (Ca^{2+} wave **[top]**; spontaneous $[Ca^{2+}]_i$ transients release **[bottom]**) from wt-PMI myocytes. **(D)** Average data of SCR occurrence from wt (n = 20 cells/4 mice), wt-PMI (n = 49 cells/8 mice), *Nod1*$^{-/-}$ (n = 24 cells/4 mice), and *Nod1*$^{-/-}$-PMI (n = 37 cells/8 mice). ***$p < 0.001$ versus wt; $^{\#\#\#}p < 0.001$ versus wt-PMI. **(E)** Representative Western blots of ryanodine receptor (RyR) and phosphorylation ryanodine receptor (P-RyR) at $Ser^{2808/2814}$ and RyR in wt, wt-PMI, *Nod1*$^{-/-}$, and *Nod1*$^{-/-}$-PMI mice. **(F)** Histograms represent the SCR occurrence in cardiomyocytes treated for 1 to 2 h with vehicle (Veh), lauroyl γ-D-glutamyl-meso-diaminopimelic acid (iE-DAP) (40 µg/ml), iE-DAP (40 µg/ml) + KT-5720 (KT) (2 µmol/l) or iE-DAP (40 µg/ml) + KN-93 (KN) (1 µmol/l). Mean ± SEM. ***$p < 0.001$ versus Veh. MI = myocardial infarction; other abbreviations as in Figures 1, 2, and 3.

We also analyzed the diastolic spontaneous Ca^{2+} release (SCR) such as Ca^{2+} waves or spontaneous $[Ca^{2+}]_i$ transients. Figure 4C illustrates 2 examples of SCR in cardiomyocytes from wt-PMI mice. The occurrence of SCR in wt-PMI cardiomyocytes was 4-fold higher than in wt cells ($p < 0.001$) (Figure 4D). However, the occurrence of SCR in *Nod1*$^{-/-}$-PMI cells was significantly lower than in wt-PMI cells and very similar to that obtained in *Nod1*$^{-/-}$ myocytes (Figure 4D). No changes were found in SCR amplitude (measured as F/F_0) or Ca^{2+} wave velocity between wt-PMI and *Nod1*$^{-/-}$-PMI cells (Online Figure 6). Supporting these data, blockade of NOD1 with nodinitib-1 in wt-PMI mice prevented the increase of the percentage of cells with SCR: 18% in wt-PMI mice treated with nodinitib-1 versus 41% in wt-PMI mice treated with vehicle ($p < 0.05$).

We determined the phosphorylation status of cardiac RyR at Ser^{2808} (primarily protein kinase A [PKA] activation site) and at Ser^{2814} (site for calcium/calmodulin-dependent protein kinase II [CaMKII] activation). Similar phosphorylation levels of RyR at Ser^{2808} and Ser^{2814} were found in *Nod1*$^{-/-}$-PMI and *Nod1*$^{-/-}$ cardiac tissue (Figure 4E, Online Figure 7), whereas wt-PMI cardiac tissue had higher levels of

phosphorylated RyR than wt tissue in both serine residues (Figure 4E, Online Figure 7). Additionally, fluorescence resonance energy transfer experiments performed in rabbit cardiomyocytes showed that the NOD1 agonist lauroyl γ-D-glutamyl-meso-diaminopimelic acid (iE-DAP) treatment increased cytosolic levels of cyclic adenosine monophosphate, a key activator of PKA and a mediator of CaMKII activation (Online Figure 8). Furthermore, cardiomyocytes incubated with iE-DAP demonstrated a significant increase of SCR that was prevented by a selective PKA inhibitor (KT-5720; Sigma, St. Louis, Missouri) or a selective CaMKII inhibitor (KN-93, Sigma) (Figure 4F). Moreover, the treatment of myocytes with KT-5720 or KN-93 also prevented the decrease in systolic calcium release and the depressed cell contractility induced by the NOD1 agonist, iE-DAP (Online Figure 9).

Next, we found that higher NOD1 protein levels coimmunoprecipitated with RyR in cardiac tissue obtained from wt-PMI versus wt, and that increased cardiac NOD1-RyR interaction in the wt-PMI group was significantly prevented by nodinitib-1 treatment (Online Figure 10A). We also analyzed whether NOD1-RyR association can rapidly regulate Ca^{2+} handling. Compared with vehicle-treated wt cardiomyocytes, cells perfused for 3 to 5 min with iE-DAP exhibited a marked decrease in $[Ca^{2+}]_i$ transient amplitude together with a significant decline in cell contraction and SR Ca^{2+} load (Online Figures 10B and 10C). Importantly, the inactive iE-DAP analogue, iE-Lys, failed to induce changes in Ca^{2+} handling.

In evaluating whether NOD1 modulated the occurrence of ventricular arrhythmias in MI mice after isoproterenol treatment, we found that spontaneous ventricular tachycardia (VT) events (Figures 5A and 5B) and mortality rates (Figure 5C) were significantly higher in wt-PMI mice than in *Nod1*$^{-/-}$ mice treated with isoproterenol.

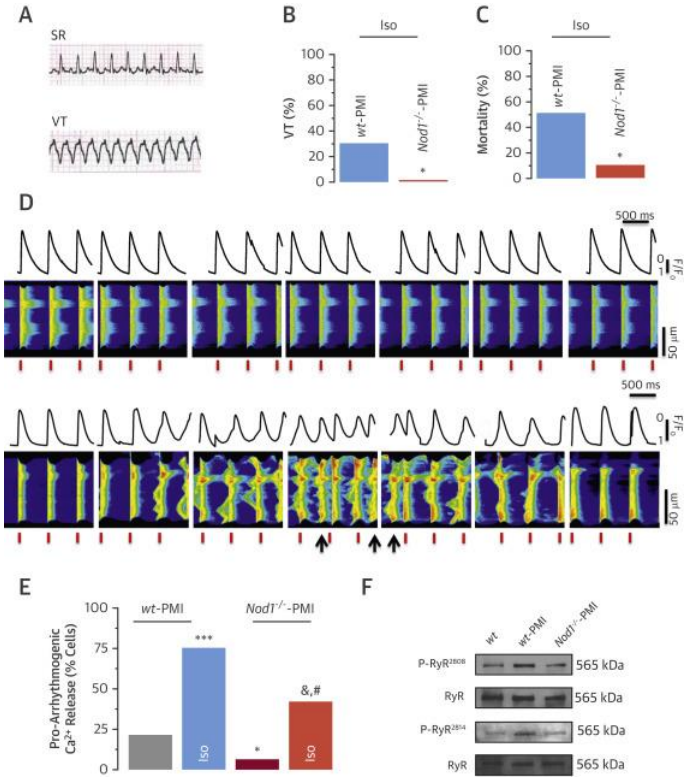

Figure 5. Antiarrhythmic Effect of NOD1 Deletion
(A) Representative electrocardiogram obtained in *Nod1*$^{-/-}$-PMI mice with normal sinus rhythm and in wt-PMI mice with ventricular tachycardia (VT) after isoproterenol (Iso) injection. Occurrence of **(B)** VT and **(C)** mortality induced after Iso treatment of wt-PMI (n = 10) and *Nod1*$^{-/-}$-PMI (n = 9) mice. **(D)** Line-scan images from wt cell paced at 2 Hz and perfused with 10^{-8} mol/l Iso **(top)**; abnormal calcium release showing multiple Ca^{2+} sparks and/or spontaneous Ca^{2+} release during pacing (**bottom; arrows** = triggered activity; **red lines** = electrical stimuli). The corresponding fluorescence intracellular Ca^{2+} concentration transients profiles appear above in each cell. **(E)** Occurrence of proarrhythmogenic Ca^{2+} release in myocytes paced at 2 Hz in the absence or presence of 10^{-8} mol/l Iso in wt-PMI (n = 28 cells/4 mice) and *Nod1*$^{-/-}$-PMI (n = 24 cells/4 mice) cells. Mean ± SEM. **(F)** Representative Western blots of P-RyR at Ser$^{2808/2814}$ and RyR in wt, wt-PMI, and *Nod1*$^{-/-}$-PMI hearts from Iso-injected mice. *$p < 0.05$, ***$p < 0.001$ versus Wt; $^{\#}p < 0.05$ vs. wt-PMI; $^{\&}p < 0.05$ versus *Nod1*$^{-/-}$. Abbreviations as in Figures 1, 2, 3, and 4.

We examined whether VT was associated with Ca^{2+} dynamics impairment at the cellular level. Figure 5D shows regular Ca^{2+} release during pacing in a wt myocyte under isoproterenol perfusion (upper panel) and a wt-PMI myocyte producing spontaneous $[Ca^{2+}]_i$ transients and after-contractions under electrical stimulation and isoproterenol administration, consistent with triggered activity (lower panel). During diastole, wt-PMI cells displayed an increase in SCR that occasionally reached the threshold to produce after-contractions and triggered activity. At baseline, the incidence of proarrhythmogenic Ca^{2+} release in wt-PMI cells was significantly higher than in *Nod1*$^{-/-}$-PMI cells (Figure 5E). Under isoproterenol stimulation, the occurrence of the proarrhythmogenic Ca^{2+} events was significantly increased in both groups; however, these events were almost 2-fold-higher in wt-PMI than in *Nod1*$^{-/-}$-PMI cardiomyocytes (Figure 5E).

We also examined RyR phosphorylation after isoproterenol administration in wt-PMI and *Nod1*$^{-/-}$-PMI hearts. The up-regulation of RyR phosphorylation at Ser$^{2808/2814}$ was significantly reduced in *Nod1*$^{-/-}$-PMI versus wt-PMI cardiac tissue (Figure 5F, Online Figure 11).

DISCUSSION

HF is a complex syndrome associated with low-grade chronic inflammation that leads to deleterious cardiac remodeling, but the underlying mechanisms are poorly understood. Here we newly identified NOD1 as a factor involved in the failing heart (Central Illustration). Pattern recognition receptor NOD1 plays a prominent role in the innate immune response to infection. Innate immune receptors can also be activated by damage-associated molecular patterns that are present in many cardiovascular disorders, including HF (11,12).

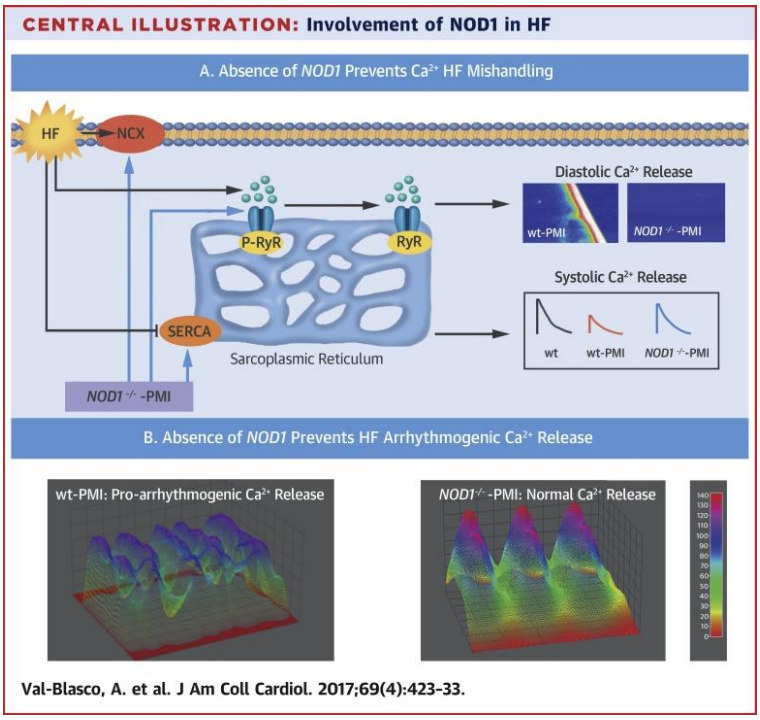

Central Illustration. Involvement of NOD1 in HF

(A) Heart failure (HF) is associated with hyperphosphorylation of ryanodine receptors (RyR) that causes an aberrant increased diastolic Ca^{2+} release as well as decreased sarcoplasmic reticulum Ca^{2+} load induced by down-regulation of the sarcoplasmic reticulum -adenosine triphosphatase (SERCA) and up-regulation of the Na^{+}/Ca^{2+} exchanger (NCX). Decreased sarcoplasmic reticulum Ca^{2+} load and increased diastolic Ca^{2+} release contribute to reduce systolic Ca^{2+} release and induce a depressed cardiomyocyte contraction. All these changes observed in wild-type post-myocardial infarction (wt-PMI) mice were blunted in *Nod1*$^{-/-}$-PMI mice, pointing to a relevant role of nucleotide-binding oligomerization domain-containing protein 1 (NOD1) in cardiac dysfunction associated with HF. **(B)** Representative 3-dimensional example of proarrhythmogenic Ca^{2+} release obtained in a wt-PMI myocyte during cell pacing (2 Hz) and a regular Ca^{2+} release obtained in *Nod1*$^{-/-}$-PMI pacing myocyte (2 Hz). P-RyR = phosphorylation ryanodine receptors.

NOD1 is ubiquitously expressed in various mammalian organs, including the heart. We showed for the first time that human failing myocardium accumulates NOD1, which is associated with increased levels of RIP2, its specific adaptor, in cardiomyocytes and increased levels of the proinflammatory factor tumor necrosis factor-α. Importantly, NOD1 levels are related to the severity of cardiac dysfunction as shown by a negative correlation between NOD1 levels and cardiac output or EF in HF patients. The higher NOD1 levels found in failing myocardium does not establish causality, but its continued presence in failing hearts suggests a mechanistic role for this protein in the pathogenesis and worsening of HF.

We used an MI-induced HF model to dissect the mechanisms by which NOD1 participates in HF progression. Similar to human tissue, the NOD1 pathway was up-regulated in failing hearts of mice and deletion of NOD1 ameliorated cardiac dysfunction as determined by echocardiography and CMR. Additionally, infarct size was smaller in *Nod1*$^{-/-}$-PMI mice than in wt-PMI mice and cardiac hypertrophy development was significantly reduced. Pharmacological blockade of NOD1 also prevents cardiac dysfunction induced after PMI. These data indicated that deletion of NOD1 prevents both functional and structural cardiac remodeling in failing hearts, pointing to a role for this pattern recognition receptor in HF progression.

Disruptions in EC coupling are well documented in almost all types of HF (9). More common changes of EC coupling associated with HF include a reduction in: 1) triggered Ca^{2+} current through L-type calcium channel (I_{CaL}); 2) systolic SR Ca^{2+} release through RyR; and 3) reuptake of Ca^{2+} into SR. All of these alterations contribute to reduce SR Ca^{2+} load, limiting the amount the SR Ca^{2+} needed to elicit regular myocyte contractions.

The possible alteration of I_{CaL} in HF is contentious. Whereas some studies have described a rise in I_{CaL}, others have reported no changes or down-regulation of these Ca^{2+} channels (13,14). Nonetheless, the majority of studies agreed that failing hearts exhibited depressed intracellular Ca^{2+} cycling and decreased SR Ca^{2+} load. Along this line, wt-PMI cells showed decreased systolic Ca^{2+} release and SR Ca^{2+} load, underlying the depressed cardiac function of wt failing animals. Importantly, *Nod1*$^{-/-}$-PMI mice exhibited an ameliorated cardiac dysfunction via an intracellular Ca^{2+} handling mechanism (vide infra). In HF, deletion of NOD1 or its pharmacological blockade prevents the decline in systolic Ca^{2+} release and in SR Ca^{2+} load. The intracellular Ca^{2+} normalization in *Nod1*$^{-/-}$-PMI mice enables cardiomyocytes to evoke regular Ca^{2+} transients and cell contractions, thereby evading, at least in part, the cardiac dysfunction found in HF. Importantly, higher NOD1-RyR association in wt-PMI cardiac tissue and the rapid regulation of Ca^{2+} handling by a NOD1 agonist support the idea of a functional role for the RyR-NOD1 association especially during HF, where this interaction increases.

SERCA is a key participant in the control of SR Ca^{2+} load uptake. Decreased SERCA activity was documented in human and experimental HF (15), and its reduced activity or expression led to impaired SR Ca^{2+} load uptake and diminished SR Ca^{2+} load, compromising systolic SR Ca^{2+} release and impairing cardiomyocyte contractility. Compared with wt, wt-PMI cells had a slower time of $[Ca^{2+}]_i$ transients together with a down-regulation of SERCA protein expression. This suggested a decreased SR Ca^{2+} uptake by the SERCA pump, correlating with the reduced SR Ca^{2+} load in wt failing cells. Conversely, NOD1 deletion prevents the impairment of the decay rates of $[Ca^{2+}]_i$ transients and SERCA down-regulation. Thus, normalization of SERCA function provoked by the deletion of NOD1 rescues SR Ca^{2+} content and might contribute to improve cell contractility, ameliorating the cardiac outcome in *Nod1*$^{-/-}$-PMI mice.

An additional essential mechanism involved in controlling $[Ca^{2+}]_i$ content is NCX. HF is associated with elevated cytosolic Ca^{2+} levels due to a decrease in Ca^{2+}-induced Ca^{2+} release and SERCA activity as described earlier, leading to a compensatory rise in NCX. Chronic up-regulation of NCX results in maladaptive cardiac remodeling because NCX does not restore SR Ca^{2+} stores, leading to potentially proarrhythmogenic events. Our data revealed that failing hearts presented higher expression of NCX protein together with a faster rate of decay of caffeine-evoked $[Ca^{2+}]_i$ transients than sham-operated hearts (wt). The constant increase in Ca^{2+} efflux derived from enhanced NCX might contribute to deplete the SR Ca^{2+} stores and depress contractility. By contrast, NCX normalization in *Nod1*$^{-/-}$-PMI cells dampens depletion of SR Ca^{2+} stores and prevents triggered activity-derived arrhythmias.

The reduction in the SR Ca^{2+} load can also be related to an increase in the Ca^{2+} leak during diastole. Indeed, several studies have reported increased diastolic Ca^{2+} release from the SR in experimental and human failing hearts (16,17). This persistent Ca^{2+} diastolic release resulted in reduced SR Ca^{2+} loading, compromising the next systolic SR Ca^{2+} release and impairing cell contraction.

We found no changes in the Ca^{2+} spark frequency in wt-PMI cells; this was corroborated by the normalization of Ca^{2+} spark frequency by the SR-Ca^{2+} load obtained in each cell and by the calculation of the overall spark-mediated Ca^{2+} leak.

Other forms of spontaneous Ca^{2+} diastolic leak (SCR) are implicated in HF, such as Ca^{2+} waves, spontaneous Ca^{2+} transients, or image-imperceptible RyR openings. The spontaneous increase in $[Ca^{2+}]_i$ might activate transient inward currents, which are assumed to be arrhythmogenic (18). Moreover, increased SCR can lead to delayed after-depolarizations and trigger arrhythmias at least in part through NCX activation; this fundamental mechanism of Ca^{2+} homeostasis in cardiomyocytes constitutes a potential substrate for certain types of arrhythmias that can be applicable to the myocardium.

Our results demonstrated a major diastolic Ca^{2+} leak in wt-PMI mice manifested as an increased occurrence of SCR events. An increase in the levels of RyR phosphorylated at PKA and CaMKII activation sites is a potential mechanism for the augmented SCR in wt-PMI mice given that chronic phosphorylation of RyR extends the open state of RyR, might promote diastolic SR Ca^{2+} leak that, in turn, depletes SR Ca^{2+} stores, and reduces EC coupling. The augmented SCR could be related to a reduction in SR Ca^{2+} load and might also promote arrhythmias. By contrast, *Nod1*$^{-/-}$-PMI myocytes have a low incidence of these aberrant events together with a normalization of RyR phosphorylation. Overall, these data showed that the prevention of increased SCR during diastole due to normalization of RyR phosphorylation in *Nod1*$^{-/-}$-PMI cells contributes to maintaining the SR Ca^{2+} content, allows regular systolic Ca^{2+} release in cardiomyocytes, and prevents triggered arrhythmias. Furthermore, in vitro experiments performed in isolated cardiomyocytes demonstrated that the selective inhibition of PKA and CaMKII prevents the increase in SCR induced by NOD1 activation, supporting a plausible mechanism by which NOD1 regulates the proarrhythmogenic spontaneous Ca^{2+} release in myocytes. Accordingly, the regulation of systolic calcium release and cell contractility by the NOD1 agonist through PKA and CaMKII, support the idea that both kinases can mediate NOD1 effects in calcium handling in our HF mice model.

HF is frequently associated with cardiac arrhythmias, particularly under β-adrenergic stimulation. Importantly, 30% to 50% of HF patients die from sudden cardiac death, and most of these deaths are linked to ventricular arrhythmias that in many cases are initiated by focal triggered activity involving Ca^{2+} handling abnormalities. We found that under β-adrenergic stimulation, wt-PMI mice, but not *Nod1*$^{-/-}$-PMI mice, developed VT resulting from Ca^{2+} handling impairment and had increased rates of sudden death presumably due to arrhythmias. These findings suggest that NOD1 deletion protects against VT. We propose that the absence of NOD1 prevents VT-derived sudden death by maintaining SR Ca^{2+} content and abnormal SR Ca^{2+} release. We corroborated these results at the cellular level, showing that wt-PMI cells under β-adrenergic stimulation had increased abnormal Ca^{2+} release under electrical stimulation that was associated with increased phosphorylation of RyR, whereas isoproterenol perfusion of *Nod1*$^{-/-}$-PMI cardiomyocytes had a significantly smaller effect in systolic abnormal Ca^{2+} release. This prevention of aberrant Ca^{2+} release in NOD1-deficient cells is associated with a normalization of RyR phosphorylation, pointing to a possible mechanism in the prevention of arrhythmias linked to *Nod1*$^{-/-}$-PMI mice.

Study limitations

NOD1 is expressed ubiquitously and although in vitro experiments are an essential tool to understand the specific role of NOD1 in the heart, the development of specific in vivo approaches will improve the knowledge of the role of this mediator in the cardiac pathophysiology.

CONCLUSIONS

Our study demonstrated that NOD1 is involved in HF progression through Ca^{2+} regulation and revealed this NLR as a new potential proinflammatory target in the treatment of HF.

Acknowledgments
The authors thank M.E. Fernández-Valle (CAI RMN RSE, UCM), V. Terrón, D. Navarro, and L. Sánchez for technical assistance; R. Madero (Section of Biostatistics of Hospital Universitario La Paz, Madrid, Spain) for help with statistical analysis; Biobank of "A Coruña" (XXIAC- Instituto de Investigación Biomédica de A Coruña) for providing us healthy heart tissue samples and the technical, ethical, and legal advice necessary for the development of our research; and A.M. Gómez for providing us the programs to analyze calcium handling.

This work was supported by grants CP11/00080 and PI14/01078 from Instituto de Salud Carlos III (ISCIII); SAF2014-52492R, SAF2014-57190R, and RTC2015-3741 from Ministerio de Economía y competitividad; Fondos Fondo Europeo de Desarrollo Regional; and Red de Investigación Cardiovascular (RIC) RD12/0042/0019. RIC is a network funded by the Carlos III Health Institute. Dr. Fernández-Velasco is Miguel Servet researcher of ISCIII. The authors have reported that they have no relationships relevant to the contents of this paper to disclose. Drs. Piedras, Ruiz-Hurtado, and Suarez contributed equally to this work.

REFERENCES

1. P.A. Heidenreich, J.G. Trogdon, O.A. Khavjou, *et al*. Forecasting the future of cardiovascular disease in the United States: a policy statement from the American Heart Association. Circulation, 123 (2011), pp. 933–944.
2. S. Frantz, L. Kobzik, Y.D. Kim, *et al.*. Toll4 (TLR4) expression in cardiac myocytes in normal and failing myocardium. J Clin Invest, 104 (1999), pp. 271–280.
3. F. Arslan, D.P. de Kleijn, G. Pasterkamp. Innate immune signaling in cardiac ischemia. Nat Rev Cardiol, 8 (2011), pp. 292–300.
4. D.L. Mann. Innate immunity and the failing heart: the cytokine hypothesis revisited. Circ Res, 116 (2015), pp. 1254–1268.
5. S. Epelman, P.P. Liu, D.L. Mann. Role of innate and adaptive immune mechanisms in cardiac injury and repair. Nat Rev Immunol, 15 (2015), pp. 117–129.
6. S. Kanno, H. Nishio, T. Tanaka, *et al*. Activation of an innate immune receptor, Nod1, accelerates atherogenesis in Apoe-/- mice. J Immunol, 194 (2015), pp. 773–780.
7. P. Prieto, M.T. Vallejo-Cremades, G. Benito, *et al*. NOD1 receptor is up-regulated in diabetic human and murine myocardium. Clin Sci (Lond), 127 (2014), pp. 165–177.
8. C. Delgado, G. Ruiz-Hurtado, N. Gomez-Hurtado, *et al.*. NOD1, a new player in cardiac function and calcium handling. Cardiovasc Res, 106 (2015), pp. 375–386.
9. E. Braunwald. The war against heart failure: the Lancet lecture. Lancet, 385 (2015), pp. 812–824.
10. R.G. Correa, P.M. Khan, N. Askari, *et al.* Discovery and characterization of 2-aminobenzimidazole derivatives as selective NOD1 inhibitors. Chem Biol, 18 (2011), pp. 825–832.
11. E. Mezzaroma, S. Toldo, D. Farkas, *et al*. The inflammasome promotes adverse cardiac remodeling following acute myocardial infarction in the mouse. Proc Natl Acad Sci U S A, 108 (2011), pp. 19725–19730.
12. M. Kawaguchi, M. Takahashi, T. Hata, *et al*. Inflammasome activation of cardiac fibroblasts is essential for myocardial ischemia/reperfusion injury. Circulation, 123 (2011), pp. 594–604.
13. I. Bodi, G. Mikala, S.E. Koch, S.A. Akhter, A. Schwartz. The L-type calcium channel in the heart: the beat goes on. J Clin Invest, 115 (2005), pp. 3306–3317.
14. F. Schroder, R. Handrock, D.J. Beuckelmann, *et al*. Increased availability and open probability of single L-type calcium channels from failing compared with nonfailing human ventricle. Circulation, 98 (1998), pp. 969–976.
15. E.G. Kranias, R.J. Hajjar. Modulation of cardiac contractility by the phospholamban/SERCA2a regulatome. Circ Res, 110 (2012), pp. 1646–1660.
16. D.M. Bers, D.A. Eisner, H.H. Valdivia. Sarcoplasmic reticulum Ca2+ and heart failure: roles of diastolic leak and Ca2+ transport. Circ Res, 93 (2003), pp. 487–490.
17. D. Terentyev, I. Gyorke, A.E. Belevych, *et al*. Redox modification of ryanodine receptors contributes to sarcoplasmic reticulum Ca2+ leak in chronic heart failure. Circ Res, 103 (2008), pp. 1466–1472.
18. J.R. Berlin, M.B. Cannell, W.J. Lederer. Cellular origins of the transient inward current in cardiac myocytes: role of fluctuations and waves of elevated intracellular calcium. Circ Res, 65 (1989), pp. 115–126.